Characterisation and magnetic field properties of multianode photomultiplier tubes

Nuclear Instruments and Methods in Physics Research A ∎ (∎∎∎∎) ∎∎∎–∎∎∎

Contents lists available at ScienceDirect

Nuclear Instruments and Methods in Physics Research A

journal homepage: www.elsevier.com/locate/nima

Characterisation and magnetic field properties of multianode photomultiplier tubes

Stephan Eisenhardt, Haofei Luo, Adam Morris, Matthew Needham, Josh Neill

University of Edinburgh, School of Physics & Astronomy, Edinburgh EH9 3JZ, UK

On behalf of the LHCb RICH Collaboration

ARTICLE INFO

Keywords:
Multianode photomultiplier tubes
Cherenkov counters
LHCb RICH

ABSTRACT

We report on studies of the Hamamatsu model R11265 Multianode Photomultiplier as part of the effort to qualify their use in the upgrade of the LHCb Ring Imaging Cherenkov Detectors. Comparisons with the known model R7600 are also made. Of particular interest is the behaviour of the MaPMT in magnetic fields comparable to the residual fringe field of the LHCb bending magnet ranging up to 25 Gauss.

1. Introduction

The upgrade of the LHCb experiment [1] will introduce 40 MHz readout to all sub-detectors. All on-detector readout electronics, currently limited to a readout rate of 1 MHz, will be replaced. Consequently, the Hybrid Photon Detectors [2] currently used in the LHCb Ring Imaging Cherenkov Detectors (RICH) [3] need to be replaced together with the readout chip [4] that is embedded in the tubes. The baseline for the photon detector replacement is the Multianode Photomultiplier R11265 from Hamamatsu [5]. For operation in LHCb the behaviour in magnetic fields is critical. The photon detectors are located within the fringe field of the LHCb dipole magnet. Even with global shielding of the photon detector boxes they are subjected to residual fields of up to 25 Gauss and may need further individual shielding.

2. MaPMT

We characterise the latest generation of MaPMT, Hamamatsu R11265, and compare to the previous generation, R7600. Both provide single photon sensitivity in the range 200–600 nm, high Quantum Efficiency of above 25% at 370 nm and a spatial resolution of better than 3 mm matching our needs. Compared to the R7600 the geometry of the R11265 has been significantly changed. This is illustrated in Fig. 1. The total active area fraction increased to 77%, compared to 50% provided by the R7600. Therefore, the R11265 may be used without lenses in LHCb RICH and still maintain a large enough photon yield. However, the redesign of the geometry also appears to cause the R11265 to be more sensitive to magnetic fields than previously established for the R7600. Notably the top and bottom row (pixels 1–8 and 57–64 in the pixel numbering scheme) turn out to be affected the most by magnetic fields. This correlates with these pixels featuring smaller pixel sizes, which are nearly 20% shorter in the direction of the entry slits, i.e. the *y*-direction of the local coordinate system, providing the room to distribute the potentials to the dynode structures. The R11265 shows better separation of the single photoelectron signal from noise (pedestal) than the R7600, which can be seen when comparing the typical signal spectra from both models, given in Figs. 2 and 3, respectively. The fits of the 1- and 2-photon contributions as well as for the photoelectron rate are modelled by Poisson distributions. Higher orders are treated with Gaussian distributions. The spectrum for the R11265 was taken at a high voltage of 800 V, i.e. 200 V below the nominal bias of 1000 V. Already at this bias the R11265 typically shows a clear valley between pedestal and 1-photoelectron contribution. Increasing the bias separates the signal further from the pedestal. The spectrum for the R7600 was taken at its nominal high voltage setting of 900 V.

Since the R11265 is clearly preferred for the larger active area and better signal-to-noise behaviour it is necessary to understand well its performance limitations in a magnetic field to evaluate its use in the LHCb RICH detectors.

3. Test setup

We use pulsed LED light with a wavelength of 470 nm and a pulse width of 15 ns to illuminate the MaPMT. We deliver the light

E-mail address: S.Eisenhardt@ed.ac.uk (S. Eisenhardt).

http://dx.doi.org/10.1016/j.nima.2014.05.036
0168-9002/

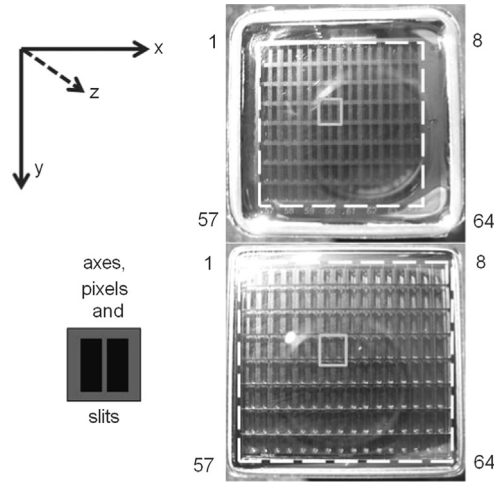

Fig. 1. Geometry of MaPMTs: entry window of R7600 (top) and R11265 (bottom); also indicated are: the total active area (approx. $(18.0\ \mathrm{mm})^2$ and $(26.0\ \mathrm{mm})^2$), the single pixel area (approximately $((2.3\ \mathrm{mm})^2$ and $(2.9\ \mathrm{mm})^2$), the orientation of the entry slits per pixel, the pixel numbering scheme and the local coordinate system.

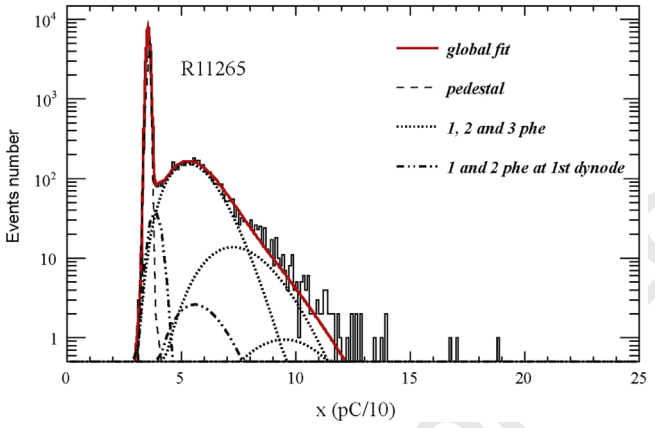

Fig. 2. Typical single photoelectron spectrum of a single pixel of a R11265, recored at HV=800 V, with Poisson fit for the photoelectron signal.

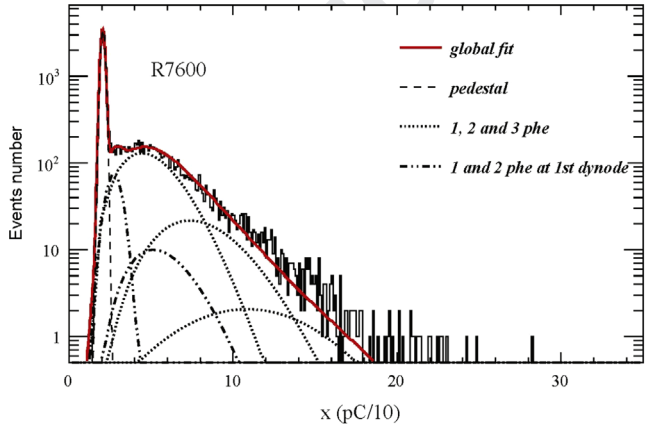

Fig. 3. Typical single photoelectron spectrum of a single pixel of a R7600, recored at HV=900 V, with Poisson fit for the photoelectron signal.

via a light guiding fibre and focus it to a spot size of ~0.1 mm using a graded index lens. The fibre end and lens are mounted on a xy-stage and illuminate one pixel at a time. This setup also allows to use Helmholtz coils which can deliver a magnetic field of up to 30 Gauss (3 mT) to the MaPMT. The entire setup is encapsulated in a dark and electrically shielded box.

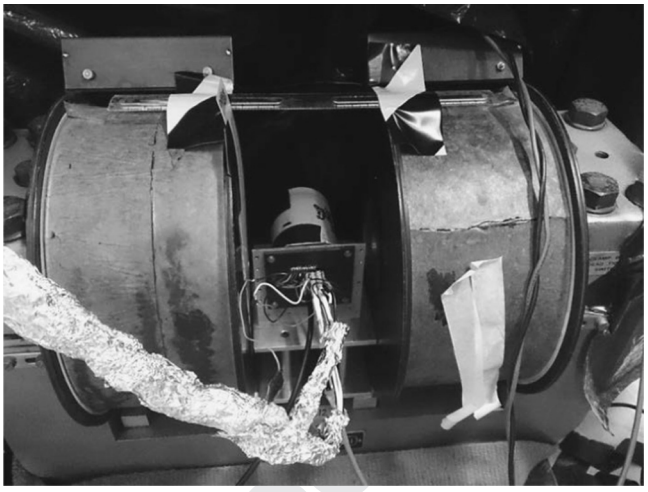

Fig. 4. Setup with small MaPMT enclosure mounted between pole shoes of stronger magnet.

Alternatively we can mount the MaPMT in a small dark cylinder, which fits into the opening of a stronger magnet, delivering fields of up to 300 Gauss (30 mT). The latter setup is shown in Fig. 4. In this small cylinder the pulsed light is delivered by the light guide entering from the back and the light reflecting diffusely off white paper fitting out the front part of the cylinder. This results in a fairly homogeneous illumination of the whole active area of the MaPMT. The intensity of the light source can be regulated to always produce spectra which are dominated by single photoelectron signals, as shown in Figs. 2 and 3. The adjustment is done online observing the single photoelectron pulses on an oscilloscope and quantified offline using the fit to a recorded signal spectrum. The intensity of the light source is sufficiently stable to neglect any variations. To match the dynamic range of the subsequent electronics the charge pulses emerging from the MaPMT are amplified by a factor $\times 100$, using a sequence of two linear amplifiers per channel, each with a bandwidth of 350 MHz and individual gains of $\times 10$. The amplified charge signals are recorded by CAEN V792 charge integrating ADCs, using a gate width of ~35 ns. Due to the limited number of available amplifiers only 16 MaPMT channels are recorded at the same time. Two connectors with a 4×2-pixel layout are used to connect to the 8×8 pin-grid-array at the base of the MaPMT. These connectors can be placed arbitrarily on the array, but for many tests it is convenient to test the four quadrants of the MaPMT in sequence. The unconnected pixels always are properly grounded to prevent internal charge-up of the anodes.

4. MaPMT characterisation and response to magnetic fields

Fig. 5 shows the signal gain across the array of pixels for the R11265 and R7600, exhibiting significantly different patterns. The R11265 has high gain in top and bottom row (pixels 1–8 and 57–64) and minimum gain in the centre, while the R7600 shows opposite behaviour. Fig. 6 shows the correlation between charge pulses of two adjacent pixels, of which only one is illuminated. Each data point represents the recorded charges for one light pulse without external magnetic field. The amount of charge found in a neighbouring channel due to cross-talk is expected to be linearly related to the charge produced in the illuminated pixel. Thus, the fitted slope of the distribution is a measure of the strength of the cross-talk. In Fig. 6 after the pedestal cut about 2000 data points are left, predominantly from single photon events. The few events with larger signal content nicely demonstrate the linearity.

Please cite this article as: S. Eisenhardt, et al., Nuclear Instruments & Methods in Physics Research A (2014), http://dx.doi.org/10.1016/j.nima.2014.05.036

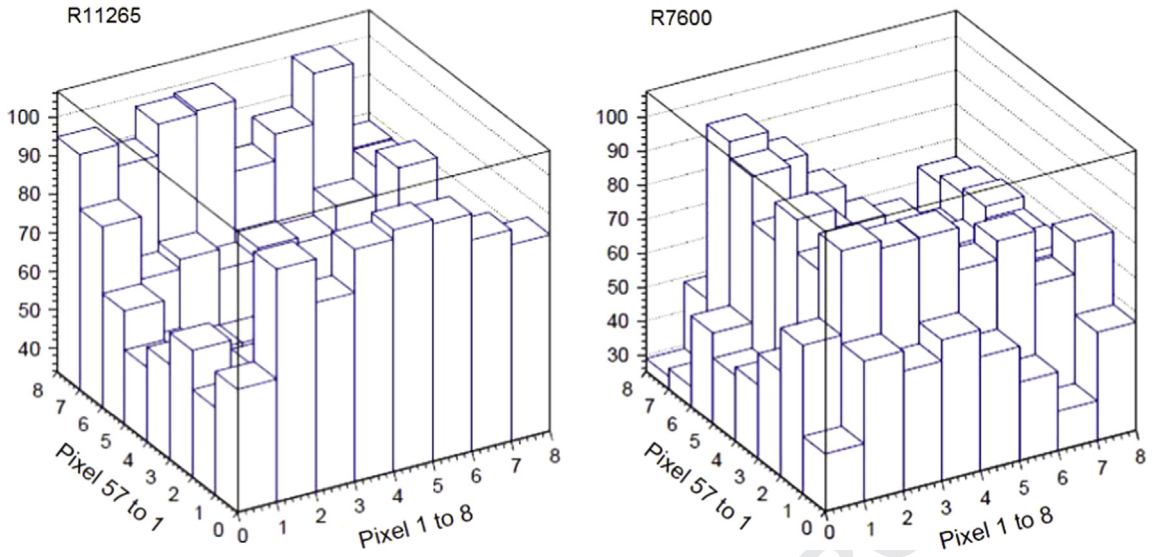

Fig. 5. Pixel-to-pixel gain variation in R11265 and R7600 without external magnetic field.

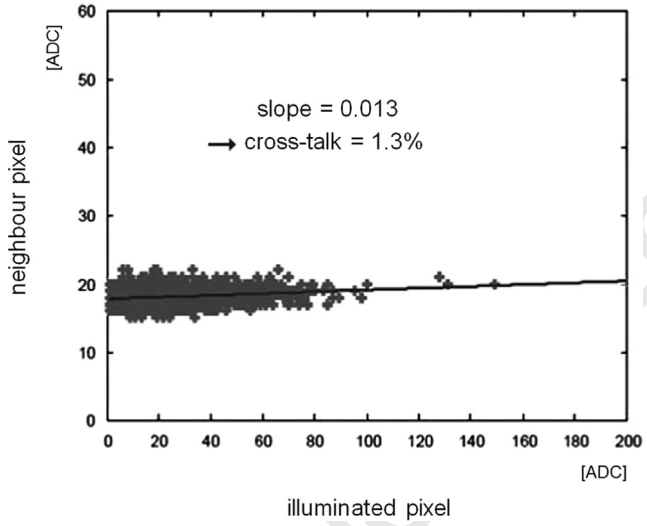

Fig. 6. Scatter plot of charge pulses in two neighbouring pixels of R11265 without external magnetic field, demonstrating the cross-talk between them. One ADC channel corresponds to 98 fC of the amplified charge pulses. A 5σ cut has been applied above the pedestal of the illuminated pixel and offset as zero, cutting away background visible in the not-illuminated channel.

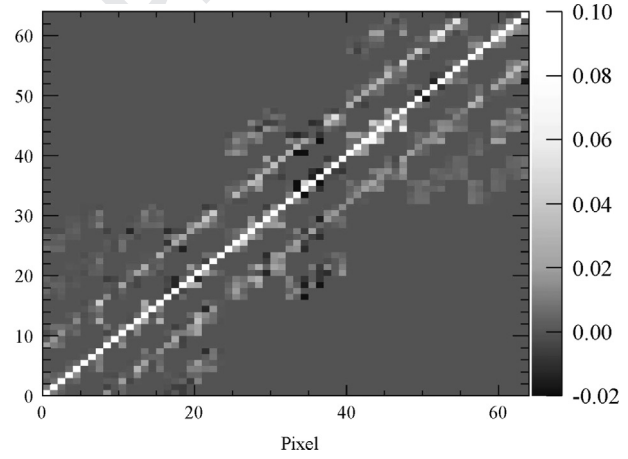

Fig. 7. Cross-talk map of R11265, without external field. The grading density is given in percent.

The R11265 shows typically cross-talk of $<2\%$ to the direct neighbours and of $<1\%$ to corner neighbours. Integrated over all 8 neighbours the typical cross-talk is $\sim 8\%$. That is larger than the integrated cross-talk of the R7600, which is typically 5%. Fig. 7 shows the cross-talk map resulting from the fits in percent for a full R11265 MaPMT. Dominantly visible are the contributions from the horizontal neighbours (± 1 in the pixel number), from the vertical neighbours (± 8) and from the diagonal neighbours (± 7 and ± 9).

Q3 Fig. 8 shows the single photoelectron efficiency of the MaPMT in dependence to magnetic fields. The efficiency is determined from the count of photons above a $5\sigma_{noise}$ threshold, typically 24 ADC channels or 23.5 fC for the signal before amplification, which turned out to be a robust measure. Data is shown for the R7600 and the R11265 with HV = 900 V and for the R11265 as well with HV = 1000 V. The red dotted lines indicate the level of 90% efficiency and ± 50 Gauss, respectively. Like the R7600 the R11265 exhibits its strongest sensitivity to magnetic field in longitudinal direction and shows a higher sensitivity in the y-direction, i.e. along the longer edge of the entry slits, than in x-direction. Overall the R11265 clearly is more susceptible to magnetic fields than the R7600. It also is seen that at lower gain the loss in efficiency due to magnetic fields is stronger. Fig. 9 displays the magnetic field strengths at which the single photoelectron efficiency drops below 90% for each pixel.[1] The larger the value, the less sensitive the pixel is. Also note the larger scale for magnetic field strength for the plots with the field in x-direction. The following additional characteristics are observed: the distinct pattern in efficiency for fields in x-, y- and z-direction, the similarity between the patterns exhibited by the R11265 and R7600 and the much stronger efficiency loss in the top and bottom row (pixels 1–8 and 57–64) compared to the other rows, most prominent with field along x- and z-direction.

5. Conclusions

We determined characteristics of the MaPMT R11265 and R7600 and find the R11265 to be affected significantly stronger

[1] Note the different orientation compared to figure Fig. 1, i.e. the top and bottom row of the MaPMT run here vertically on the sides.

Please cite this article as: S. Eisenhardt, et al., Nuclear Instruments & Methods in Physics Research A (2014), http://dx.doi.org/10.1016/j.nima.2014.05.036

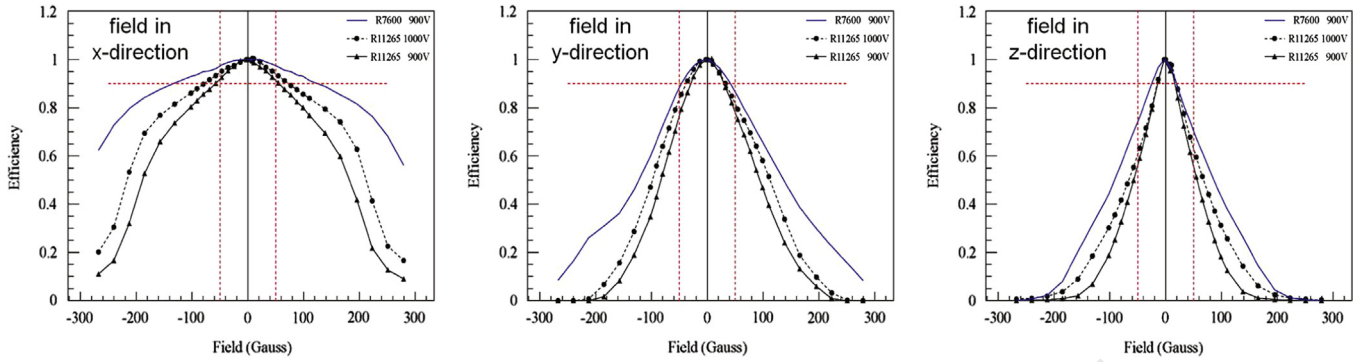

Fig. 8. Single photoelectron efficiency of MaPMT in dependence to magnetic fields along the three axes, averaged over all pixels and normalised to zero field. (For interpretation of the references to color in this figure caption, the reader is referred to the web version of this paper.)

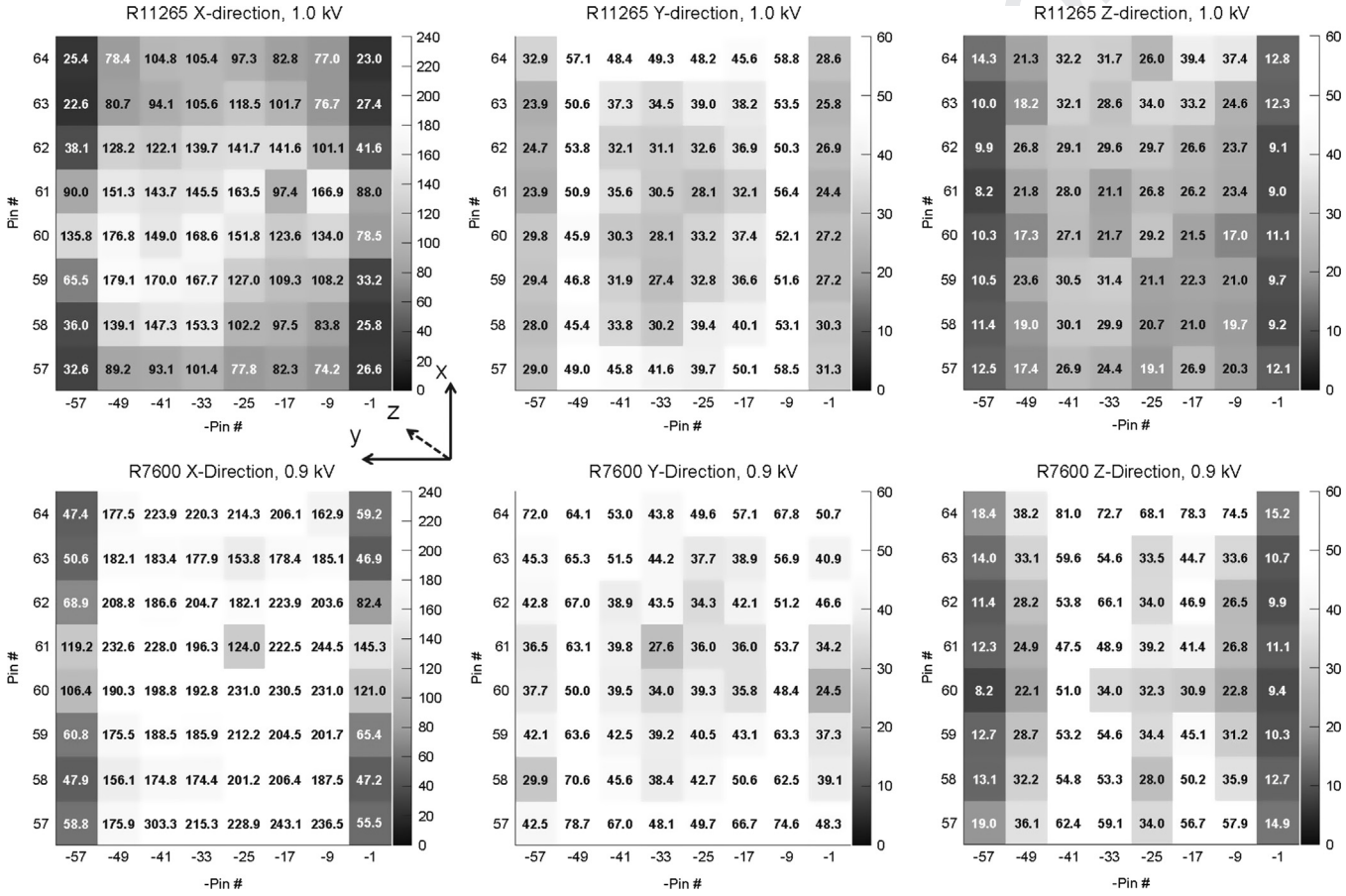

Fig. 9. Magnetic field strength maps for 90% single photoelectron efficiency of MaPMT, in Gauss, which are viewed from the back and are rotated compared to Fig. 1. Note the larger scale for the measurements with field in the *x*-direction.

by magnetic fields than the R7600. Particularly the loss of efficiency in the top and bottom rows suggests the need for individual mu-metal shields in fields of up to 25 Gauss. Similar for both models is their relative behaviour to the orientation of the external magnetic field. Longitudinal fields, along the tube axis (*z*-direction), cause the largest degradation in the efficiency to recognise single photo electrons. The MaPMT are most robust against fields oriented along the short axis of the entry slits of the pixels (*x*-direction). As the model R11265 can be operated at larger high voltage some of the additional signal loss with respect to the model R7600 can be recovered by an increase of the operating voltage.

References

[1] I. Bediaga, et al., Framework TDR for the LHCb Upgrade: Technical Design Report; The LHCb Collaboration, CERN/LHCC-2012-007, LHCb-TDR-12-2012.
[2] M. Alemi, et al., Nuclear Instruments and Methods in Physics Research Section A 449 (2000) 48.
[3] A. Augusto, et al., The LHCb Collaboration, Journal of Instrumentation 3 (2008) S08005.
[4] K. Wyllie, et al., A pixel readout chip for tracking at ALICE and particle identification at LHCb, in: Proceedings of the Fifth Workshop on LHC Electronics, Snowmass, CO, USA, 20–24 September 1999. CERN/LHCC/99-33.
[5] I. Bediaga, et al., LHCb Particle Identification Upgrade: Technical Design Report; The LHCb Collaboration, CERN/LHCC-2013-022, LHCb-TDR-14-2013.

Please cite this article as: S. Eisenhardt, et al., Nuclear Instruments & Methods in Physics Research A (2014), http://dx.doi.org/10.1016/j.nima.2014.05.036